

# Characterization of bubble mobility during flow through fibrous porous media

Shih Wen Chen<sup>1,2</sup> (✉), Navid Niknafs Kermani<sup>1,2</sup>, Pavel Simacek<sup>1,2</sup>, Suresh G. Advani<sup>1,2</sup>

1. Center for Composite Materials, University of Delaware, Newark, DE 19716, USA

2. Department of Mechanical Engineering, University of Delaware, Newark, DE 19716, USA

## Abstract

Multiphase flow through porous media is a common phenomenon during the processing of composite materials in which viscous liquid thermoset resin containing small bubbles due to entrapped air is injected into reinforcing porous fibrous media. The composite part is formed once the resin cures. Entrapped bubbles cause porosity, which is characteristic of materials fabricated by this technique and results in reduced mechanical properties. Hence, the reduction in porosity during the processing stage remains a critical issue. To investigate this, an experimental study was conducted to characterize the movement of bubbles within the pore network of the fabric's weave architecture representing the porous media. Bubble dynamics, as the simulated resin impregnated the fibrous network, were observed in transparent molds for three fabric architectures, with bubble diameter and velocity being measured as they traversed through the fabric. A dimensionless number is introduced to correlate the fabric weave architecture to the bubble size, revealing that higher bubble mobility (indicating how fast the bubble moves compared to the pore averaged resin velocity) is observed in tighter weaves and with larger bubbles. To predict bubble mobility based on bubble size and fabric weave, two physics-based models are introduced. The predicted results are compared with the experimental data, facilitating void minimization by regulating bubble mobility.

## Keywords

multiphase flow  
porous media  
bubble dynamics  
fabric weave  
void minimization

## Article History

Received: 25 April 2024

Revised: 1 August 2024

Accepted: 16 August 2024

## Research Article

© The Author(s) 2026

## 1 Introduction

Multiphase flow of liquids and gases in the form of bubbles through porous media is indeed a phenomenon encountered in various fields, including the processing of composite materials. The movement of multiple phases (liquid and air) through porous media is usually affected by the applied pressure gradient and capillary and viscous forces (Agaoglu et al., 2015; Blunt, 2001; Bogdanov et al., 2011; de Boer, 2000; Patel et al., 2019; Wang, 1988; Wood and Bader, 1994; Yang and Lu, 2021). In multiphase flow through porous media, different phases move differently in response to pressure gradients. Capillary forces play an important role in regulating the phase distribution within such heterogeneous porous media. Additionally, viscosity plays a role in the relative motion of phases, with less viscous fluids tending to migrate faster due to reduced resistance to flow (Agaoglu et al., 2015; Bear and Bachmat, 1990; Bogdanov et al., 2011;

de Boer, 2000; Dullien, 1975; Patel et al., 2019; Wood and Bader, 1994).

In the context of composites, porous media refer to fiber reinforcement during the manufacturing of the composite by the liquid composite molding (LCM) process. LCM encompasses a group of composite manufacturing processes, where resin is injected into a sealed mold containing dry fabric to occupy the empty spaces between the fibers. Once the resin reaches the vent, injection is discontinued, and upon curing of the resin, the composite part is demolded (Advani and Sozer, 2010; Sozer et al., 2000). The liquid is usually a viscous thermoset resin (approximately 200–500 times more viscous than water), which contains tiny undesirable air bubbles. These air bubbles become voids when they become trapped within the composite as the resin cures and solidifies. To maintain the mechanical properties of cured composite parts, many manufacturers strive to limit the void content to less than 1%–2% (Gangloff et al.,

✉ shihwen@udel.edu

## Nomenclature

$A$	cross-sectional area of the bubble ( $\text{m}^2$ )	$Re$	Reynolds number
$C_d$	drag coefficient of bubble	$U$	bubble mobility/mobility factor
$D$	diameter of the spherical bubble (m)	$v$	velocity of the fluid (m/s)
$F_b$	buoyancy force ( $\text{kg}\cdot\text{m}/\text{s}^2$ )	$v_B$	velocity of the bubble by Darcy's law (m/s)
$F_d$	drag force ( $\text{kg}\cdot\text{m}/\text{s}^2$ )	$v_{\text{bubble}}$	velocity of the bubble (m/s)
$H$	gap length between the fabric tows (m)	$v_f$	volume averaged velocity of fluid (m/s)
$h$	height between two parallel plates (m)	$v_{\text{fluid}}$	pore averaged velocity of fluid (m/s)
$K$	permeability of the medium ( $\text{m}^2$ )	$v_r$	relative velocity (m/s)
$L$	length of tubing (m)	$V_w$	average velocity of the entire gap region (m/s)
$L_b$	length of cylindrical bubble (m)	$\mu$	viscosity of the fluid (Pa·s)
$L_c$	length of the fabric tow channel (m)	$\rho_f$	density of the fluid ( $\text{kg}/\text{m}^3$ )
$Q$	volume flow rate ( $\text{m}^3$ )	$\nabla P$	pressure gradient (Pa/m)
$R$	pipe radius (m)	$\Delta P$	pressure difference between inlet and outlet (Pa)
$r$	radius of the bubble (m)		

2015; de Almeida and dos S. N. Neto, 1994; Yang and Lu, 2021). Voids can compromise the mechanical characteristics of composites by promoting microcracking, primarily due to stress concentrations initiated by voids, leading to premature fatigue failures (Gangloff et al., 2015; Varna et al., 1995; Liu et al., 2006; Wood and Bader, 1994; Yang and Lu, 2021; Dutra et al., 2021). To effectively control the behavior of voids, it is essential to understand the relation between resin flow, bubble dynamics and the architecture of porous media (Li et al., 2024).

Void formation in LCM processes can be attributed to various factors. The two dominant ones would be (i) the entrapment of air or other volatiles during the flow of resin and (ii) insufficient infusion speed leading to gelation before infiltration is finished (Mehdikhani et al., 2019; Pillai, 2002; Pupin et al., 2017; Rabaud et al., 2011). The former is usually the dominant factor unless the infusion is poorly planned. The presence of air and volatiles in the mold stems from insufficient evacuation prior to the infusion, moisture, or other volatiles dissolved in the resin or even as a result of chemical reactions during the curing process.

The volatiles dissolved within the resin nucleate into bubbles with dropping pressure, or bubbles are already present within the resin as it enters the mold (Chui et al., 1997). They are transported with resin and show intricate dynamics of their own. The intent is to accelerate them, so they reach the flow front during the filling stage and are evacuated through the vent in the properly designed infusion process. The motion of bubbles is influenced by a number of parameters.

Buoyancy refers to the force from the pressure gradient observed between the inlet and outlet of the fluid system under vacuum. This pressure gradient is due to the inlet

pressure being higher than the vacuum pressure at the outlet. This pressure differential provides the forward force on the bubbles. The vertical component (buoyancy force due to gravity) of this gradient is quite small compared to the horizontal part. This pressure gradient clearly drives the bubble to move *faster than the resin*. The magnitude of this speed-up is uncertain *but crucial since this allows bubbles to evacuate through the resin flow front*. The role of capillary forces and physical constraints within the reinforcement pores is not determined (Patel and Lee, 1995). To understand and characterize bubble movement, we conducted an experimental investigation of bubble motion during resin flow in porous media.

In our study, we investigate the motion of discrete bubbles utilizing a concept known as bubble mobility, denoted as  $U$  (Patel and Lee, 1995; Gangloff et al., 2014a, 2014b). The characterization of bubble mobility represents a fundamental component in our analysis of the transport phenomena. Bubble mobility refers to the ability of bubbles in a liquid to move or migrate within that medium (Mehdikhani et al., 2019; Pupin et al., 2017). It is a characteristic that describes how fast the bubble moves relative to the average fluid velocity (Mehdikhani et al., 2019; Pupin et al., 2017).

In cases involving multidimensional flow configurations, bubble mobility is tensorial in nature, as it couples the vector of fluid velocity—in our case, pore averaged—with the vector of bubble velocity. The two may be generally misaligned. In our work, we simplify the flow behavior (one-dimensional flow). To this end, the reinforcement will be aligned with the flow, and the symmetry will keep the velocities of the fluid and bubble aligned. In that case, the bubble mobility (mobility factor) can be defined as a scalar

as the ratio of the velocity of the bubble divided by the averaged pore velocity of the fluid,  $v_{\text{fluid}}$  which is defined as the volume flow rate/(cross-sectional area\*porosity) (Eq. (1)):

$$U = \frac{v_{\text{bubble}}}{v_{\text{fluid}}} \quad (1)$$

Thus, we will investigate this ratio and its dependence on several factors: bubble size, resin viscosity, and reinforcing fabric geometry. The bubbles that either entered the resin or were formed due to local flow disturbances cannot reach the flow front and vent unless  $U$  is greater than unity (Mehdikhani et al., 2018; Lee et al., 2006; Song and Hu, 2017; Leclerc and Ruiz, 2008; Patel et al., 1993; Olsson and Kreiss, 2005; Yang and Lu, 2021).

This condition, however, may not be entirely sufficient to ensure their successful removal. As the resin flow can be modeled and the velocity field computed (Gangloff et al., 2014a), the determination of bubble mobility allows one to track a bubble inserted into the field and *determine* whether it will reach the advancing resin front or be “left behind”, creating micro- or meso-level porosity (Gangloff et al., 2015; Mehdikhani et al., 2018). Tracking multiple bubbles would allow one to determine potential locations where this porosity accumulates.

In this work, we first experimentally characterize the bubble velocities as they flow through different fabric architectures. Next, we correlate the fabric weave to the bubble size and then introduce models to predict bubble mobility based on bubble size and fabric weave and compare the results with the experimental data. We have presented a schematic outlining the structure and our approach to address the objective of this work in Fig. 1.

## 2 Experimental setup

This study aims to examine the relationship between bubble mobility and the inherent attributes of both the bubble and the porous medium it traverses through. To achieve this, the fabric weave is placed in a closed rectangular mold with transparent plates to facilitate and record the flow of the carrying fluid and the bubbles through the porous medium. The injection of the bubble is automated with the syringe driven by constant displacement at the inlet tube. The experimental procedure is elaborated upon in Section 2.1.

### 2.1 Experimental procedure

In this study, to facilitate the flow through the porous media, a vacuum at the outlet generates the required pressure gradient to drive the flow through the porous media within a closed mold. Corn syrup is selected as the surrogate fluid due to its ease of viscosity adjustment, which greatly enhances its operational efficiency. The mold is fabricated using two transparent acrylic plates (20.5" × 6"). A 1/32" rubber seal is used to prevent any leakage around the plates, while clamps are employed to securely fasten the mold plates in place. The rubber seals help provide control over the fiber volume fraction within the mold. Figure 2 presents a schematic of the experimental setup.

For enhanced visualization of bubble dynamics within the fabric, a single-layer fabric (11 cm × 10 cm) is placed inside the mold, directly beneath an overhead-mounted camera. Bubbles are consistently generated at the inlet using an automatic syringe. The size of the bubbles is controlled by the size of the syringe needle, as presented in Table 1.

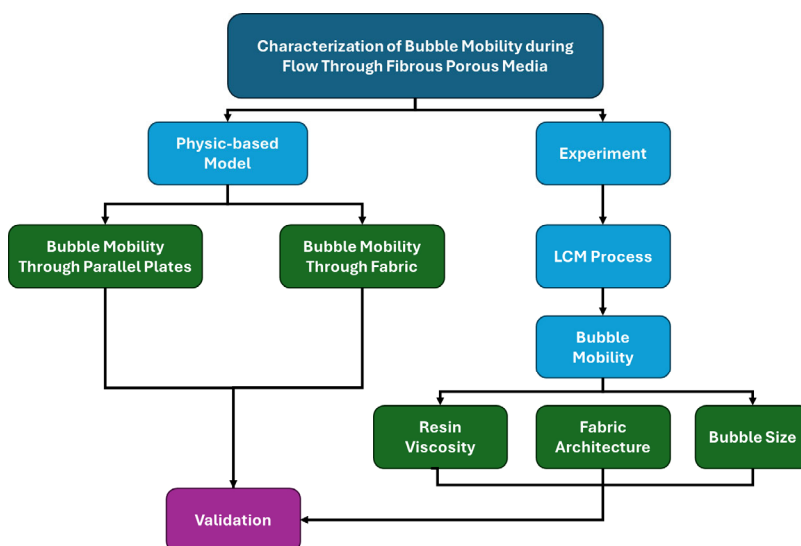


**Fig. 1** Schematic of the approach to investigate the role of bubble mobility in fibrous porous media.

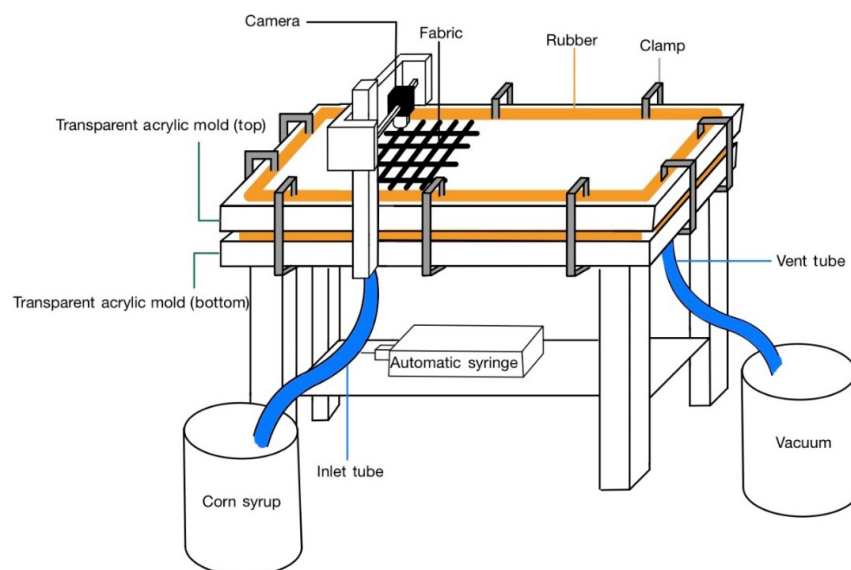


**Fig. 2** Schematic of the experimental setup to monitor bubbles moving through the fabric (porous media) during the injection process (Chen et al., 2023). The setup consists of two transparent acrylic molds with a rubber spacer. Fabric is placed between the inlet and outlet ports. The automatic syringe that is connected to the inlet tube creates bubbles of various sizes that depend on its diameter.

**Table 1** Size of the utilized needles in the experiments and their corresponding generated bubble diameters upon entry which is defined as the in-plane diameter

Inner needle diameter (mm)	0.06	0.09	0.16	0.33
Bubble diameter (mm)	0.40–2.00	1.50–2.50	2.00–3.50	3.00–5.00

## 2.2 Materials and measurements

One primary objective of this study is to systematically investigate the influence of different fabric types and weave patterns on bubble mobility within fibrous porous media. Accordingly, experiments are conducted employing a range of distinct fabric types detailed in Table 2.

To ensure a consistent fluid flow velocity and prevent disruptive phenomena such as “racetracking”, which involves the resin traveling at higher speeds along fabric edges due to imperfect fabric fit along the mold walls, clay was applied

along the lateral edges of the mold, as shown in Fig. 3(A). This effectively eliminates racetracking and promotes a uniform flow from the inlet to the vent.

To determine the fiber volume fraction within Region II (Fig. 3(B)), the fiber volume was calculated by weighing the fabric and dividing it by the total volume of Region II, which was calculated by measuring the gap between the acrylic plates. Furthermore, a vacuum test was conducted to ensure that there were no leaks within the mold before proceeding to open the inlet to let in the fluid.

To calculate the bubble velocity, measurements were taken in three distinct regions, as depicted in Fig. 3(B). The schematic presented in Fig. 3(B) highlights three regions within the mold: the space (i) between the inlet and the fabric (Region I), (ii) occupied by the fabric (Region II), and (iii) between the fabric and the vent (Region III). These regions were chosen strategically to capture various

**Table 2** List of the fabrics used in the experiments

Fiber type	Glass	Glass	Carbon	Carbon
Weave patterns	Plain	Mock Leno	Plain	Twill
Brand	ACP Composites	ACP Composites	Sigmatex	Sigmatex
Weight	9.6 oz/yd <sup>2</sup>	20.10 oz/yd <sup>2</sup>	8.85 oz/yd <sup>2</sup>	12.09 oz/yd <sup>2</sup>
Fabric schematic				

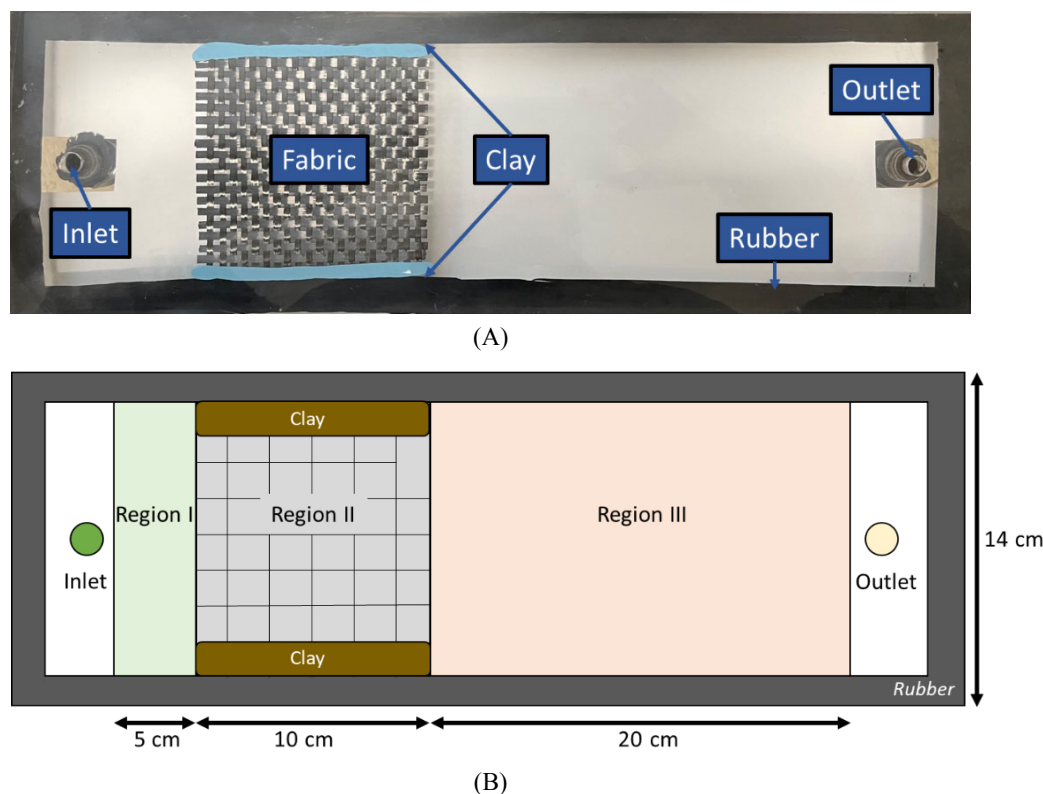


**Fig. 3** (A) Top view of the experimental setup. (B) Schematic of the setup shows three regions within the mold: (i) Region I: between the inlet and the fabric, (ii) Region II: fabric, and (iii) Region III: between the fabric and the vent (outlet).

aspects of bubble motion and its relationship with local flow characteristics. However, this investigation primarily concentrates on the bubble motion within the first two regions.

The dynamic alteration in bubble size is a consequence of the pressure drop across the mold length and constitutes a significant facet of our investigation. It is imperative to note that the measurement of bubble dimensions is conducted at the point of entry into the mold. In addition to the bubble size variations observed during entry, it is essential to acknowledge the presence of a pressure drop inherent in both the inlet and the outlet tube. The pressure drop in these tubes can be calculated by using the Hagen-Poiseuille equation, which is shown below. These are usually quite small and are neglected.

$$\Delta P = \frac{8\mu QL}{\pi R^4} \quad (2)$$

where  $\Delta P$  is the pressure difference between the two ends,  $\mu$  is the viscosity of the fluid,  $Q$  is the volume flow rate,  $L$  is the length of the tubing, and  $R$  is the pipe radius.

To attain the desired viscosity, water is added to the corn syrup in precise proportions, and the mixture is thoroughly blended to ensure uniformity. Subsequently, the viscosity of this mixture is measured using a digital viscometer

(Brookfield DV-I) to confirm that it aligns with the required specifications.

Achieving accurate observation and analysis of bubble motion during the flow monitoring experiment requires precise camera positioning. This involves aligning the camera to capture the intended view, often referred to as the region of interest (ROI) within the mold. Figure 4 presents the ROI of the camera, specifically showcasing the transition of a bubble flowing through from Region I to Region II and finally entering Region III by moving through the channels in the fabric. Figure 4 illustrates the change in the shape of the bubble as it enters the porous media. Our focus is on individual bubble motion rather than broader phenomena such as bubble clusters or the flow patterns of bubble trains moving through fibrous porous media. This focused approach allows us to thoroughly examine the characteristics and behavior of this particular bubble type. By analyzing factors such as its size, we can gain a deeper understanding of its interactions within the experimental context.

This experiment was conducted in which the inlet was at atmospheric pressure and a vacuum was applied at the outlet. The bubble size in the experiments was measured before it entered the fabric by using the image tool where we placed a ruler that indicated the bubble's size in relation to it. The increase in bubble diameter ranged between

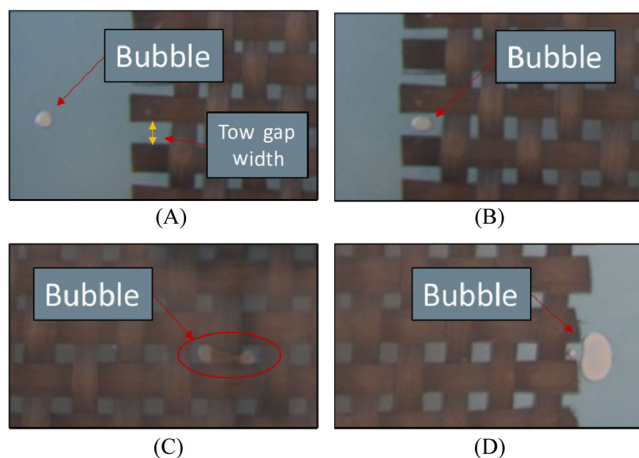


**Fig. 4** The location of the bubble through the fabric: (A) before the bubble enters the fabric in Region I, (B) bubble at the entrance of the Region II entering tow gap, (C) bubble traveling through the gap between fiber tows in Region II, (D) bubble exiting from the gap into Region III.

10.3% and 23.2% as it progressed through the fabric due to the decreasing pressure. However, it is important to note that for our analysis, we neglect any variations in bubble size caused by the pressure gradient.

The pore-averaged flow velocity was determined by measuring the mass flow rate using a precision weighing scale and assessing the fiber volume fraction relative to the rubber thickness. Consequently, the calculation of the mobility factor for each bubble in different regions was facilitated by measuring bubble velocity through captured images by the camera (Eq. (1)).

### 2.3 Experimental results

In the conducted experiments, bubble mobility was

systematically assessed over a range of bubble diameters by introducing various fabric weaves into the mold. The primary orientation of these fabrics was aligned with the direction of fluid flow. Figure 5 displays the measured data for bubble diameters before entering the fabric (Region I) with respect to the width of the measured fabric's channel gap between the tows, through which the bubbles traverse in the specific fabrics employed throughout the experiments.

As shown in Fig. 5, bubbles with different diameters were introduced for each type of fabric. The range of bubble diameters remained relatively consistent, typically between 0.25 and 5 mm at incoming pressure (close to 1 atm). Notably, the tow gap width in the plain carbon fiber fabric was observed to be greater than that in the Twill and Mock Leno fabrics.

This is followed by measuring the mobility factor of each bubble, defined as the ratio of bubble velocity to pore averaged flow velocity (Eq. (1)), across various experiments that are shown in Fig. 6. The scatter in the data were due to the measurement errors in bubble size and velocity and the variability introduced by the variation within the fabric architecture and the nesting between the various fabric layers. To investigate the physics associated with the bubble mobility factor during its passage through the porous medium, this parameter is measured both in a region devoid of the porous media (Region I) and within the porous media itself (Region II). From Fig. 6, one can observe a substantial difference in the mobility factor of bubbles flowing through these two regions.

Figure 6 reveals that the bubble mobility in Region I is notably restricted (remaining between 0.4 and 2). In contrast, the mobility factor increases by an order of magnitude when bubbles move through the fabric. This is because of the effect of bubbles on the physics of flow. In Region I, the

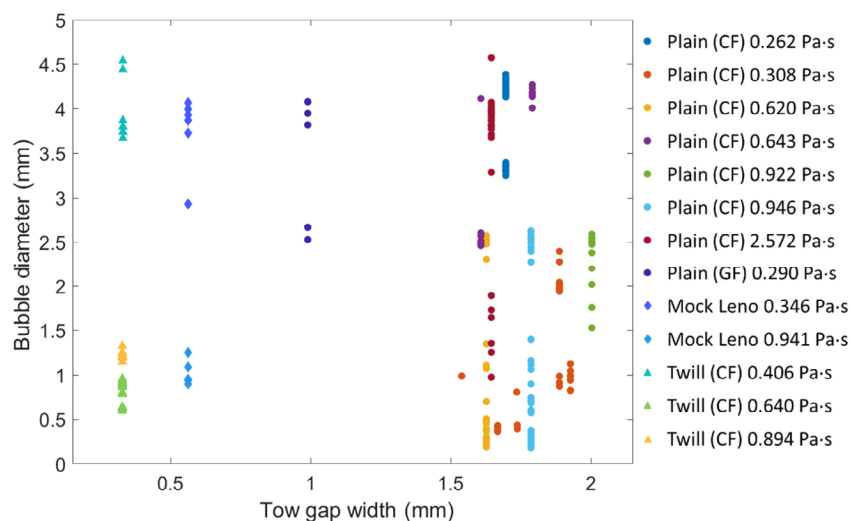


**Fig. 5** Bubble size and tow gap width variations for various fabric weave patterns as listed in Table 2 for each experiment. The viscosity of the simulated resin in each experiment is provided in the legend.

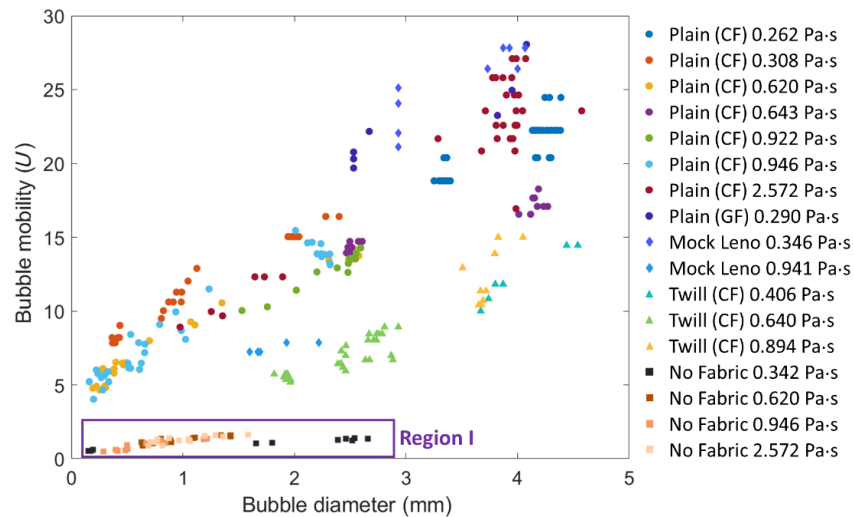


**Fig. 6** Measured bubble mobility is presented as a function of bubble diameter in each experiment including both in Region I (no-fabric with  $0.4 < U < 2$ ) and Region II (fabric groups as listed in Table 2). The viscosity of the resin in each experiment is in the legend.

bubbles are small relative to the flow domain and do not impact the flow. In Region II—assuming that the bubble is comparable with the channel size—the presence of bubbles impacts the flow in *that channel by reducing viscous drag*. The bubble does not move faster than the fluid (capillary forces add only a slight increase (Bretherton, 1961)), but the fluid moves much faster in that individual channel than the pore average value suggests, and the bubble just rides along with it.

### 3 Proposed bubble mobility models

The experimental results suggest two distinct physics associated with the mobility factors of bubbles when they travel through (i) the region between the plates without the porous media (Region I) and (ii) the region within the porous media (Region II). In this section, two physics-based models are proposed to predict the mobility factor of bubbles traveling through these two regions.

#### 3.1 Bubble mobility between thin parallel plates (Region I)

To propose a physics-based model to predict the velocity of a bubble moving within a thin gap between two solid mold plates, the primary assumptions made are as follows. (i) The buoyant and drag forces are the only forces that are exerted on the bubbles. (ii) These forces are equal and opposite, so there is no net force on the bubble, and hence, the bubble does not experience any acceleration in this region. (iii) No-slip boundary conditions exist on the mold plate surfaces. Note that for gaseous bubbles, the mass is negligible and so would be the inertia forces (acceleration being instant).

In flows driven by an applied pressure gradient, as depicted in Fig. 7, pressure gradient  $\nabla P$  is mostly aligned with flow and results in a similarly aligned buoyancy force as described in Eq. (7) (Imberger, 2013):

$$F_b = \frac{4}{3} \pi r^3 \nabla P \quad (3)$$

where  $F_b$  is the buoyancy force and  $r$  is the radius of the bubble. Moreover, the drag force acting on the bubble is a function of its size, shape, and the velocity of the fluid, which can be formulated as Eq. (4) (Liu et al., 2006):

$$F_d = \frac{1}{2} \rho_f C_d A v^2 \quad (4)$$

where  $F_d$  is the drag force,  $\rho_f$  is the density of the fluid,  $C_d$  is the drag coefficient,  $A$  is the cross-sectional area of the bubble, and  $v$  is the velocity of the fluid. The drag coefficient is typically determined using empirical equations based on experimental data (Dey et al., 2019). The sphere is one of the most commonly studied shapes for this purpose.

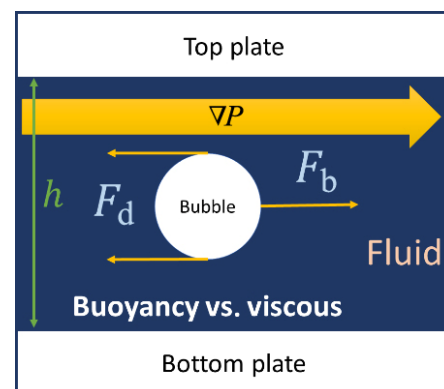


**Fig. 7** Model I—Bubble mobility between thin parallel plates.

The relationship between the drag coefficient and the Reynolds number ( $Re$ ) (Dey et al., 2019):

$$Re = \frac{\rho_f v D}{\mu} \quad (5)$$

where  $\rho$  is the fluid density,  $v$  is the flow velocity,  $D$  is the diameter of the sphere, and  $\mu$  is the viscosity of the fluid. In the experiments conducted in this study, the density and viscosity of the corn syrup are characterized by values of  $1.20 \text{ g/cm}^3$  and  $0.26\text{--}2.57 \text{ Pa}\cdot\text{s}$ , respectively. The velocity of bubbles within Region I is on the order of  $2 \text{ mm/s}$ , resulting in Reynolds numbers  $\sim 0.1$ . A theoretical formula for the drag coefficient of a sphere at Reynolds numbers below  $0.2$  was developed by George Gabriel Stokes and is presented in Eq. (6) (Khalaf, 2009).

$$C_d = \frac{24}{Re} \quad (6)$$

By substituting Eq. (6) into Eq. (5), the relationship in Eq. (7) provides the expression for the drag force exerted on a sphere moving within a fluid with relative velocity  $v_r$ :

$$F_d = 3\mu\pi D v_r \quad (7)$$

Hence, if a bubble is in a state of constant velocity without experiencing acceleration ( $\sum F = 0$ ), within a fluid, the relationship between the relative velocity ( $v_r$ ), the pressure gradient, and the bubble diameter can be determined by equating the buoyancy force (Eq. (4)) with the drag force (Eq. (6)):

$$v_r = \frac{1}{18} \frac{\nabla P D^2}{\mu} \quad (8)$$

The relative velocity of the bubble ( $v_r$ ) with respect to the average velocity of the fluid ( $v_f$ ) can be described as  $v_r = v_b - v_f$ , where  $v_b$  is the velocity of the bubble. In our work, the fiber volume fraction is over  $47\%$ , and it has been shown that with this fiber volume fraction, Darcy's law is valid for low Reynold numbers ( $< 0.2$ ). Using Darcy's law (Eq. (9)) (Whitaker, 1986), one can describe the average velocity of the fluid ( $v_f$ ) as a function of the permeability of the medium ( $K$ ).

$$v_f = \frac{-K}{\mu} \nabla P \quad (9)$$

The permeability of the channel between two parallel plates with a height denoted as ( $h$ ) can be estimated as  $h^2/12$ . Consequently, by rearranging Eq. (8) with regard to the definition of the pressure gradient according to Darcy's law and the permeability of the channel, the mobility factor of a bubble (as defined in Eq. (1)) can be

expressed as Eq. (10):

$$U = 1 + \frac{2D^2}{3h^2} \quad (10)$$

One of the assumptions in the proposed model can be modified due to the limitation in image processing in the experiment. From the experimental setup, all images are captured from the top view. Therefore, the location of the bubbles through the thickness of the channel between the two parallel plates is not known with certainty. In the proposed model, it is assumed that the bubble moves within the flow in the middle, equal distance from the top and the bottom plate. However, in reality, smaller bubbles might touch the top plate due to the buoyancy effect, as schematically shown in Fig. 8.

As a result, the average flow velocity within the region traversed by the bubble deviates from the initially proposed model, and it can be corrected by computing the average flow velocity in close proximity to the plate at a distance  $D$  as Eq. (11):

$$\begin{aligned} V_B &= \frac{3}{2} V_w \frac{1}{D} \int_{\frac{h}{2}-D}^{\frac{h}{2}} \left[ 1 - \left( \frac{2y}{h} \right)^2 \right] dy \\ &= V_w \left[ \frac{3D}{h} - 2 \left( \frac{D}{h} \right)^2 \right] \end{aligned} \quad (11)$$

where  $V_B$  is the average velocity of the bubble region and  $V_w$  is the average velocity of the entire gap region. Once again, through the rearrangement of Eq. (8) in accordance with Darcy's law and the permeability of the channel, it becomes possible to express the corrected mobility factor for a bubble moving between two plates (Region I).

$$U = \left[ 1 + \frac{2 \left( \frac{D}{h} \right)^2 \left[ \frac{3D}{h} - 2 \left( \frac{D}{h} \right)^2 \right]}{\left[ \frac{3D}{h} - 2 \left( \frac{D}{h} \right)^2 \right]} \right] \quad (12)$$

In Section 4, the predictions regarding the bubble mobility

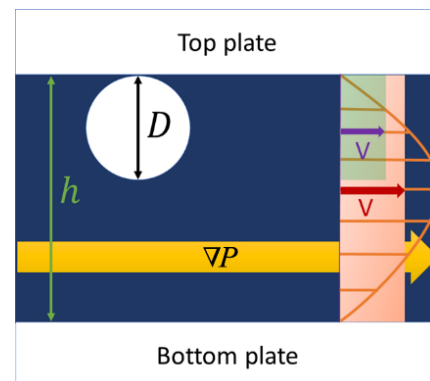


**Fig. 8** Region I—Smaller bubbles ascend and touch the top plate and its average velocity is corrected by averaging it over distance  $D$  instead of distance  $h$  in the modified model.

factor, as derived from this initial formulation, will be subjected to a comparative analysis with the measured experimental data.

### 3.2 Bubble mobility through porous media (Region II)

To develop a physics-based model aimed at predicting the mobility factor of bubbles as they permeate a porous medium (fabric), it is postulated that the principal physics governing this phenomenon is the pressure gradient across the bubble. In our work, the textile reinforcement could be represented by a large number of parallel “tubes” that are periodically connected by transverse channels that allow pressure equalization. The averaged or pore averaged (apparent) velocity of fluid is averaged over all of the parallel channels as it is proper to do so for the textile reinforcement. The bubble length is comparable to the channel size, and we assume that in this particular channel, the bubble moves with the fluid. As a result, any effects stemming from bubble fragmentation and capillary pressure are intentionally neglected. This could lead to slight differences in the results (< 10% correction for the capillary effects) (Bretherton, 1961) but in comparison with flow velocity in the majority of channels without bubbles (quite possibly 10× slower).

To account for the changes in the bubble’s shape during its transit through the fabric (as depicted in Fig. 4), it is assumed that the bubble, when within the fabric, takes on a cylindrical form of length,  $L_b$ . Figure 9 provides an illustrative representation of a bubble traversing the fabric tow channel length,  $L_c$ . As shown in Fig. 9, the diameter of the reshaped bubble within the fabric channel is equal to the gap between the fabric tows ( $H$ ). Hence, Eq. (13) is formulated to equate the volume of the bubble prior to entering the fabric with the volume of the reshaped bubble, serving to facilitate the computation of the elongated bubble’s length within the fabric.

$$\text{Bubble volume} = \frac{\pi}{6}D^3 = \frac{\pi}{4}L_bH^2 \quad (13)$$

The schematic presented in Fig. 9 illustrates the pressure gradient ( $P_2 - P_1$ ) within the upper channel, without bubbles, which facilitates the application of Darcy’s law for the determination of the volume-averaged flow velocity within this channel (as expressed in Eq. (14)).

$$v_f = \frac{K \Delta P}{\mu L_c} \quad (14)$$

where  $K$  is the permeability of the channel within the fabric that the bubble moves through. However, if it is presumed that the pressure remains constant within the bubble, the

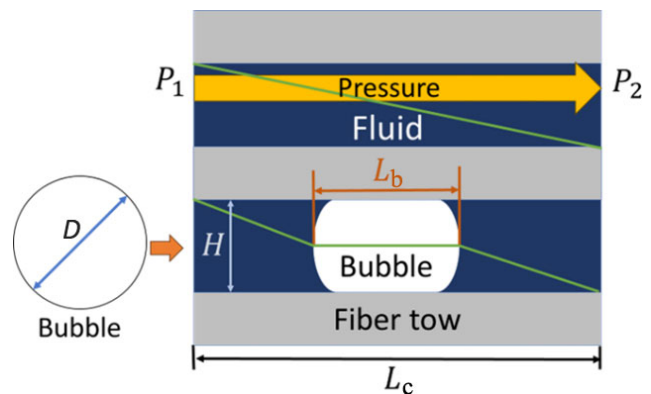


**Fig. 9** Schematic of bubble mobility through the porous fabric. The green line shows the pressure drop along the channel.

volume-averaged flow velocity within the channel containing the bubble can be expressed as Eq. (15):

$$v_B = \frac{K \Delta P}{\mu L_c - L_b} \quad (15)$$

Similar to the preceding model, the mobility factor of the bubbles can be formulated by rearranging Eqs. (13)–(15) with respect to the relative velocity of the bubble.

$$U = \frac{1}{1 - \frac{2}{3} \left( \frac{D}{H} \right)^2 \left( \frac{D}{L_c} \right)} \quad (16)$$

Nevertheless, two specific limitations are inherent in this model. First, it necessitates that the bubble possesses an initial diameter exceeding the width of the fiber tow gap to ensure contact with the tow channel following elongation. Second, the length of the bubble is constrained from exceeding the length of the channel itself. In Section 4, the comparison of the predicted mobility factors with the experimental data will be discussed in detail.

## 4 Results and discussion

### 4.1 Factors impacting bubble mobility

In Fig. 6, the measured mobility factors were described with respect to the diameter of bubbles before they entered the fabric. However, the information discerned from the figure primarily pertains to the disparity in mobility factors between bubbles within Region I and those within Region II. To enable a comparative analysis of bubble mobility across various fabric weave types, a dimensionless parameter was introduced by dividing the bubble diameter by the tow gap width ( $D/H$ ), as shown in Fig. 10. This approach allowed for the normalization of the measured experimental data in relation to the fabric characteristics, thereby facilitating a

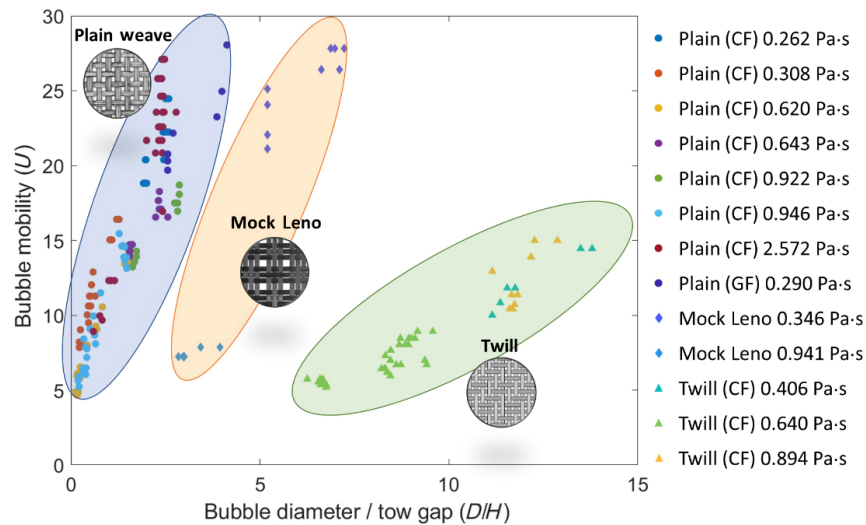


**Fig. 10** Effect of bubble diameter to tow gap width ratio on bubble mobility in Region II.

qualitative assessment of the influence of the fabric type on the mobility factor of bubbles.

Figure 10 illustrates the classification of the measured data by plotting the mobility factor of bubbles with respect to the dimensionless number of  $(D/H)$  in Region II. The utilization of this nondimensional number provides a clear understanding of the dependency of the mobility factor on the fabric's architectural characteristics, specifically in relation to the tow gap width. Fabrics characterized by smaller bubble size to tow gaps or denser packing of fiber tows ratio  $(D/H)$  tend to exhibit lower bubble mobility within the same type of weaving fabric.

Figure 11 displays the measured mobility factor of bubbles in experiments employing a carbon fiber plain weave. This presentation helps in identifying the influence of various parameters on bubble mobility.

For the results illustrated in Fig. 11, the parameters under consideration encompass viscosity and the dimensionless number  $(D/H)$ . It can be deduced that viscosity exerts a relatively minor influence on bubble mobility, given the similarity in the mobility factor of bubbles when viscosity is altered by an order of magnitude, ranging from 0.26 to 2.57 Pa·s. Furthermore, Fig. 11 elucidates the impact of bubble diameter on the mobility factor. Within the findings presented in Fig. 11, an equivalent tow gap measurement was employed in the construction of the dimensionless number. Consequently, a higher dimensionless value signifies a larger bubble diameter. Despite the scatter in the results due to the measurement errors in bubble size and velocity and the variability introduced by the variation within the fabric architecture and the nesting between the various fabric layers, these results show that larger bubbles, present before entering the fabric, exhibit an elevated mobility factor as they move through the fabric.

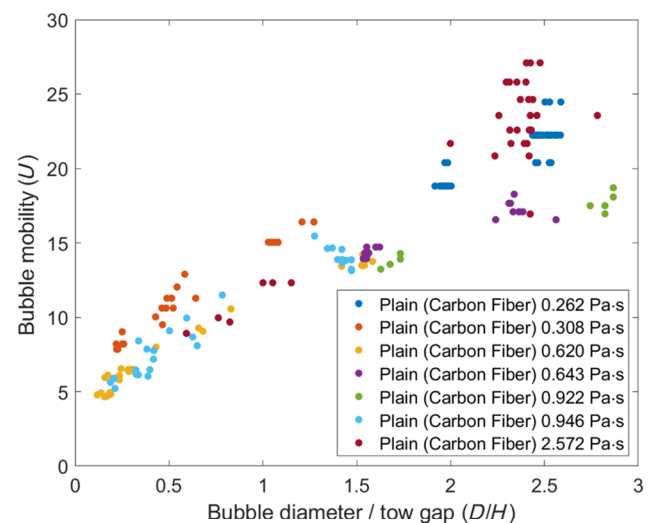


**Fig. 11** Effect of bubble diameter to tow gap width ratio on bubble mobility with different fluid viscosities for plain weave carbon fiber experiments.

## 4.2 Model validation

In this section, the experimentally measured mobility factor of bubbles is compared to the values predicted by the proposed physics-based models. First, as presented in Fig. 12, the proposed model for the bubbles moving between two parallel plates separated by a gap of height  $h$  (Region I) is compared with the experimental data.

There is very good agreement for larger bubbles or higher  $(D/h)$  with the model. However, when the ratio of bubble diameter to gap height falls below 0.5, the experimental data do not align satisfactorily with the model. However, in the modified model, accounting for the vertical buoyancy force causing the bubble to ascend adjacent to the top plate,

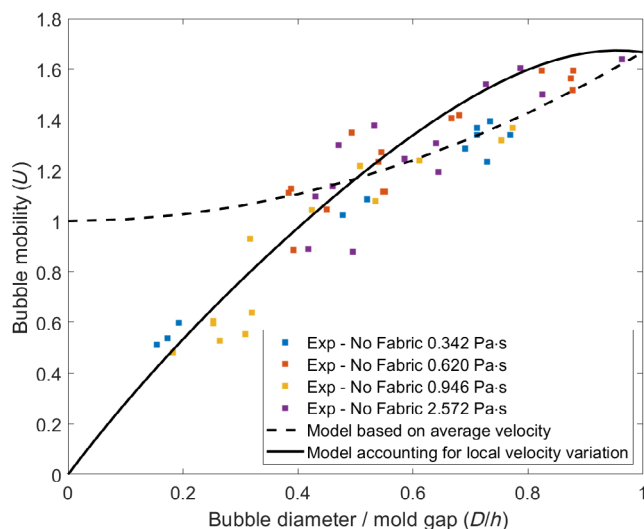


**Fig. 12** Comparison of mobility predictions (Eq. (10)) with experimental data of bubble flow between parallel plates. The dotted line is for the model that does not account for smaller bubble sizes than the distance between the plates. The model accounts for local velocity variation is more accurate for smaller bubble sizes.

a remarkable improvement in the agreement between the experimental data and the model is found in Fig. 12.

Finally, the model proposed for Region II to predict the mobility factor of bubbles traversing through the porous media channels is compared with experimentally obtained data in Fig. 13. It is important to note that this comparison encountered two specific limitations stemming from the model's assumptions. First, for this comparison, the selected bubbles should have been sufficiently large to ensure that the diameter of their elongated form was comparable with the width of the channel. Additionally, the length of the elongated bubble should have been constrained to be shorter than the length of the channel between the fabric tows. Within the constraints of these two limitations, Fig. 13 illustrates a notable alignment between our model and the experimental data, indicating a strong correlation.

We observe a discrepancy between the experimental data and the model, and this variance can be attributed to our consideration of bubble size exclusively upon entry. In reality, the bubbles expand as the pressure decreases through the porous media. Larger bubbles inherently possess greater bubble mobility, leading to an augmented impact on the flow dynamics. The model's divergence from the experimental data highlights the need for a more nuanced incorporation of dynamic bubble size changes in response to pressure drops within the porous media to achieve a more accurate representation of the system behavior.

## 5 Conclusions

This study focused on investigating the movement of bubbles

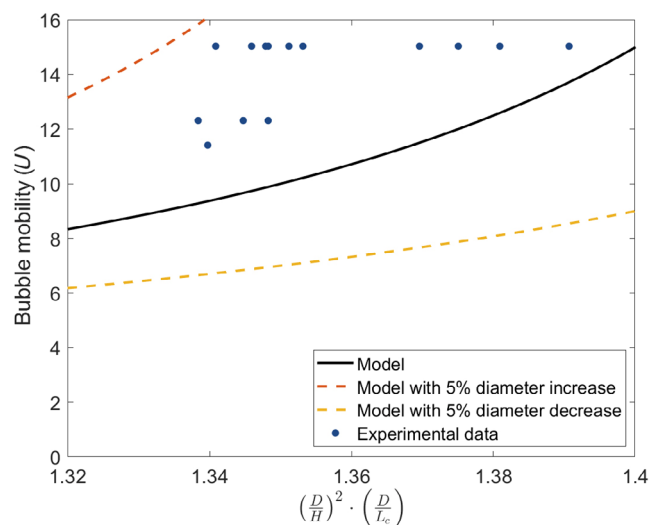


**Fig. 13** Comparison of mobility predictions (Eq. (16)) with experimental data—Flow through fabric reinforcement.

within the flow through porous media. The primary objective was to assess the effect of parameters such as bubble size, porous media characteristics, and viscosity on the mobility factor of bubbles that represent how fast the bubbles move relative to the average resin velocity through the porous media. To achieve this, an experimental setup was designed and constructed specifically for monitoring bubble dynamics during fluid flow through fibrous porous media in a sealed mold. This setup featured two transparent acrylic molds, and bubbles were introduced at the inlet and tracked using a camera. Each experiment utilized a single-layer fabric as the porous medium, with three different weave types: (i) plain carbon and glass fiber weave, (ii) Twill, and (iii) Mock Leno weave.

From the experimental data, it was observed that the bubble mobility was approximately an order of magnitude lower between two parallel plates compared to when bubbles had to traverse through the porous fabric. Furthermore, the experimental results show that when considering the influence of viscosity in relation to fabric weave type, it did not exert a significant impact on bubble mobility. The introduced dimensionless number, which is defined as the ratio of bubble diameter to fabric tow gap width, exhibited a strong correlation with bubble mobility across various fabric weave types. Notably, bubbles with similar dimensionless numbers within the same fabric architecture displayed similar mobility characteristics, allowing for the classification of results into distinct clusters for different fabric types. Additionally, a comparative analysis of the experimental data revealed that larger bubbles tended to exhibit higher mobility within the same fabric structure.

Our study also presented two simple physics-based models that estimate bubble mobility based on flow parameters in the two regions. The first model predicts the mobility factor

of a bubble as it moves within a flow between two parallel plates in the absence of fibers, accounting for buoyancy and drag forces. The equation based on buoyancy and drag forces for a bubble based on averaged flow velocity proved grossly overestimating the mobility for small bubbles. In response to this discrepancy, a modified estimate that accounts for the nonuniformity of the velocity field between plates was proposed, which rectified the shortcoming, resulting in very good agreement with the experimentally measured data.

Then, for Region II, the mobility of bubbles in the porous media was investigated under simplifying assumptions, such as disregarding contact forces and neglecting bubble fragmentation. Despite these limitations, our model indicates good agreement with the experimental data.

Thus, this work has shed light on the role of several material and process variables on bubble mobility through a porous fabric. First, the bubble mobility depends on the bubble size and has been measured to be much higher than what has been reported in the literature. Second, the viscosity of the fluid does not seem to have a strong influence on bubble mobility, and third, we show that the type of fibrous porous media architecture influences bubble mobility. Finally, we also introduce simple models to describe the bubble mobility and compare it with our experimental measurements.

While the experimental findings and physics-based models presented in this study rely on certain assumptions, they provide a valuable starting point for future research into bubble mobility within porous media. The observed results can be utilized in potential practical applications in the removal of trapped bubbles during the manufacturing of composite parts.

## Acknowledgements

The present work is funded by the US National Science Foundation (NSF), Award No. 2023323, which is gratefully acknowledged by the authors.

## Declaration of competing interest

The authors have no competing interests to declare that are relevant to the content of this article.

## References

- Advani, S. G., Sozer E. M. 2010. *Process Modeling in Composites Manufacturing*, 2nd edn. CRC Press.
- Agaoglu, B., Copty, N. K., Scheytt, T., Hinkelmann, R. 2015. Interphase mass transfer between fluids in subsurface formations: A review. *Advances in Water Resources*, 79: 162–194.

- Bear, J., Bachmat, Y. 1990. Mass transport of multiple fluid phases under isothermal conditions. In: *Introduction to Modeling of Transport Phenomena in Porous Media*. Dordrecht: Springer Netherlands: 327–398.
- Blunt, M. J. 2001. Flow in porous media—Pore-network models and multiphase flow. *Current Opinion in Colloid & Interface Science*, 6: 197–207.
- Bogdanov I., Kpahou J., Kamp A. 2011. Direct pore-scale modeling of two-phase flow through natural media. In: Proceedings of the COMSOL Conference.
- Bretherton F. P. 1961. The motion of long bubbles in tubes. *Journal of Fluid Mechanics*, 10(2): 166–188.
- Chen, S. W., Niknafs, N., Simacek, P., Advani, S. G. 2023. Experimental investigation of bubble mobility in porous media during resin transfer molding. In: Proceedings for the American Society for Composites-38th Technical Conference.
- Chui, W. K., Glimm, J., Tangerman, F. M., Jardine, A. P., Madsen, J. S., Donnellan, T. M., Leek, R. 1997. Case study from industry: Process modeling in resin transfer molding as a method to enhance product quality. *SIAM Review*, 39: 714–727.
- De Boer, R. 2000. Contemporary progress in porous media theory. *Applied Mechanics Reviews*, 53: 323–370.
- De Almeida, S. F. M., dos Santos Nogueira Neto, Z. 1994. Effect of void content on the strength of composite laminates. *Composite Structures*, 28: 139–148.
- Dey, S., Zeeshan Ali, S., Padhi, E. 2019. Terminal fall velocity: The legacy of Stokes from the perspective of fluvial hydraulics. *Proceedings of the Royal Society A: Mathematical, Physical and Engineering Sciences*, 475: 20190277.
- Dullien, F. A. L. 1975. Single phase flow through porous media and pore structure. *The Chemical Engineering Journal*, 10: 1–34.
- Dutra, C. M. B., Amico, S. C., Souza, J. A. 2021. Evaluation of flow-mesh influence in resin injection processes. *Applied Composite Materials*, 28: 369–380.
- Gangloff, J. J., Daniel, C., Advani, S. G. 2014a. A model of two-phase resin and void flow during composites processing. *International Journal of Multiphase Flow*, 65: 51–60.
- Gangloff, J. J., Hwang, W. R., Advani, S. G. 2014b. Characterization of bubble mobility in channel flow with fibrous porous media walls. *International Journal of Multiphase Flow*, 60: 76–86.
- Gangloff, J. J., Hwang, W. R., Advani, S. G. 2015. The investigation of bubble mobility in channel flow with wavy porous media walls. *International Journal of Multiphase Flow*, 70: 1–14.
- Imberger J. 2013. Chapter 4 - Effect of viscosity. In: *Environmental Fluid Dynamics*. Academic Press, 181–218.
- Khalaf H. K. 2009. The theoretical investigation of drag coefficient and settling velocity correlations. Master Thesis. Nahrain University.
- Leclerc, J. S., Ruiz, E. 2008. Porosity reduction using optimized flow velocity in Resin Transfer Molding. *Composites Part A: Applied Science and Manufacturing*, 39: 1859–1868.
- Lee, D. H., Lee, W. I., Kang, M. K. 2006. Analysis and minimization of void formation during resin transfer molding process. *Composites Science and Technology*, 66: 3281–3289.
- Li, C., Zhou, H., Sun, Y., Sun, F., Liu, Z., Huang, J., Zhang, L., Yue, C., Zhao, Q., Yu, S., et al. 2024. Research on the influence of yarn



- reduction on the bending performance of three-dimensional woven composites. *Applied Composite Materials*, 31: 1069–1082.
- Liu, L., Zhang, B. M., Wang, D. F., Wu, Z. J. 2006. Effects of cure cycles on void content and mechanical properties of composite laminates. *Composite Structures*, 73: 303–309.
- Mehdikhani, M., Gorbatiikh, L., Verpoest, I., Lomov, S. V. 2019. Voids in fiber-reinforced polymer composites: A review on their formation, characteristics, and effects on mechanical performance. *Journal of Composite Materials*, 53: 1579–1669.
- Olsson, E., Kreiss, G. 2005. A conservative level set method for two phase flow. *Journal of Computational Physics*, 210: 225–246.
- Patel, H. V., Kuipers, J. A. M., Peters, E. A. J. F. 2019. Effect of flow and fluid properties on the mobility of multiphase flows through porous media. *Chemical Engineering Science*, 193: 243–254.
- Patel, N., Lee, L. J. 1995. Effects of fiber mat architecture on void formation and removal in liquid composite molding. *Polymer Composites*, 16: 386–399.
- Patel, N., Rohatgi, V., Lee, L. J. 1993. Influence of processing and material variables on resin-fiber interface in liquid composite molding. *Polymer Composites*, 14: 161–172.
- Pillai, K. M. 2002. Governing equations for unsaturated flow through woven fiber mats. Part 1. Isothermal flows. *Composites Part A: Applied Science and Manufacturing*, 33: 1007–1019.
- Pupin, C., Ross, A., Dubois, C., Rietsch, J. C., Vernet, N., Ruiz, E. 2017. Formation and suppression of volatile-induced porosities in an RTM epoxy resin. *Composites Part A: Applied Science and Manufacturing*, 94: 146–157.
- Rabaud, D., Thibault, P., Raven, J. P., Hugon, O., Lacot, E., Marmottant, P. 2011. Manipulation of confined bubbles in a thin microchannel: Drag and acoustic Bjerknes forces. *Physics of Fluids*, 23: 042003.
- Song, K., Hu, X. 2017. Modeling self-assembly and capture phenomenon of two droplets in high aspect ratio microchannels. *Computers & Fluids*, 144: 10–18.
- Sozer, E. M., Bickerton, S., Advani, S. G. 2000. On-line strategic control of liquid composite mould filling process. *Composites Part A: Applied Science and Manufacturing*, 31: 1383–1394.
- Varna, J., Joffe, R., Berglund, L. A., Lundström, T. S. 1995. Effect of voids on failure mechanisms in RTM laminates. *Composites Science and Technology*, 53: 241–249.
- Wang, C. Y. 1998. Modeling multiphase flow and transport in porous media. In: *Transport Phenomena in Porous Media*. Amsterdam: Elsevier: 383–410.
- Whitaker, S. 1986. Flow in porous media I: A theoretical derivation of darcy's law. *Transport in Porous Media*, 1: 3–25.
- Wood, J. R., Bader, M. G. 1994. Modelling the behaviour of gas bubbles in an epoxy resin: Evaluating the input parameters for a diffusion model using a solubility parameter approach. *Journal of Materials Science*, 29: 844–850.
- Yang, W., Lu, S. 2021. Modeling of void formation based on non-isothermal conditions in liquid composite molding for plain-weave fabric. *Fibers and Polymers*, 22: 1466–1481.

**Open Access** This article is licensed under a Creative Commons Attribution 4.0 International License, which permits use, sharing, adaptation, distribution and reproduction in any medium or format, as long as you give appropriate credit to the original author(s) and the source, provide a link to the Creative Commons license, and indicate if changes were made.

The images or other third party material in this article are included in the article's Creative Commons license, unless indicated otherwise in a credit line to the material. If material is not included in the article's Creative Commons license and your intended use is not permitted by statutory regulation or exceeds the permitted use, you will need to obtain permission directly from the copyright holder.

To view a copy of this license, visit <http://creativecommons.org/licenses/by/4.0/>.